Annealing temperature Dependent on Morphology and Electrochemical Properties of ZnFe₂O₄ Nanoparticles Synthesized by Sol-Gel Method

Lixia Liao[1,2], Tao Fang[1], Geping Yin[3], Dongxi Zhang[1], Bin Li [1,2]*

[1] Department of Chemistry, College of Science, Northeast Forestry University, Harbin 150040, China
[2] Post-doctoral Mobile Research Station of Forestry Engineering,
Northeast Forestry University, Harbin 150040, China
[3] School of Chemistry and Chemical Engineering, Harbin Institute of Technology, Harbin, 150001, China
[*]E-mail: lxliao1024@126.com, libinzh62@163.com

A series of ZnFe₂O₄ nanocrystals were synthesized by sol-gel method. The surface morphology, structure and the electrochemical performace of the materials annealed in the temperature range of 500-800°C were characterized by X-ray diffraction(XRD), scanning electron microscopy(SEM), Multipoint N₂ adsorption-desorption experiment, constant current charging-discharging test, cyclic voltammetry(CV) and electrochemical impedance spectroscopy(EIS) techniques. Consequently, the morphology and electrochemical performance of these materials are very sensitive to the sintering temperature. ZnFe₂O₄ material treated at 600°C exhibits the initial reversible capacity of 1384.4 mAh g^{-1} and retains the highest capacity of 622 mAh g^{-1} after 50 cycles. The superior electrochemical performance is attributed to its smaller charge transfer resistance of 43.9 Ω and higher lithium ion diffusion coefficient of 2.01×10^{-15} cm² s^{-1}, which due to the morphology with the smaller particle size and higher dispersibility.

1. INTRODUCTION

With the decreasing of fossil fuels and intensifying of urban environment pollution, study on electric vehicles also becomes very urgent and important. Battery is one of key parts in electrical vehicle. Traditional graphite anode used in commercial lithium ion batteries can not satisfy the demand of power battery, owing to its low theoretical capacity (only about 372 mAh g^{-1}) and the safety

problem that arises with Li-metal deposition on graphite up on fast-charge of lithium ion battery. Intensive research effort toward alternative anode materials has been inspired. Zinc ferrite ($ZnFe_2O_4$) was applied in various application fields due to superior light, electricity, gas sensitivity and electric magnetic properties, but the electrochemical performance as lithium ion battery anode materials was becoming attentive only in recent decades, owing to high theoretical capacity of about 1000 mAh g[-1][1]. Different strategies for preparing Zn-ferrites[2-6] were obtained, and the electrochemical performance is remarkably different by adopting various synthesis methods and preparation conditions. Sintering temperature was one of important factors influencing electrochemical performance, however the investigations were mainly focused more on the morphology design of material and the corresponding electrochemical performance by optimizing heated temperature, and the essential reason of that the influence of annealing temperature on electrochemical performance of $ZnFe_2O_4$ was quite unclear.

In this study, $ZnFe_2O_4$ nanocrystals were obtained by citric acid assisted sol-gel technique followed by annealing at the temperature range of 500-800°C. The structure and electrochemical performance of $ZnFe_2O_4$ electrode sintered at various temperatures were characterized, and the corresponding kinetic behavior of the $ZnFe_2O_4$ electrode was analyzed.

2. EXPERIMENTAL

2.1 Material preparation and characterization

All chemicals were of analytical grade and were used without further purification. The materials were prepared by sol-gel technique. Ferric nitrate nonahydrate($Fe(NO_3)_3 \cdot 9H_2O$) and zinc nitrate hexahydrate ($Zn(NO_3)_2 \cdot 6H_2O$) where the mole ration is 2:1 were dissolved in de-ionized water and poured into a beaker followed by the addition of equimolar amount of citric acid. Ammonia was added to the mixture till the pH reached 7. The above solution was under magnetic stirring at about 70°C for 6 h. During heating process, water was gradually vaporized and a gel was formed. And finally the cooled gel was annealed at various temperatures in muffle furnace, and a brown $ZnFe_2O_4$ nanomaterial was obtained. The $ZnFe_2O_4$ materials sintered at 500, 600, 700 and 800°C were labeled as ZF-500, ZF-600, ZF-700 and ZF-800.

The surface morphology was observed by the scanning electron microscopy(Hitachi S4700). The crystal structure of the as-prepared products was analyzed by X-ray diffraction (XRD; PANalytical X'Pert PRO, Cu Kα radiation), and the crystallite size was calculated using the Scherrer formula: $D=0.89\lambda/\beta\cos\theta$, where D is the crystal size in nm, λ is the X-ray wavelength in nanometer (0.15406 nm for Cu-Kα), β is the half-width of the diffraction peak in rad, and θ is the corresponding diffraction angle. Multipoint N_2 adsorption-desorption experiment was carried on an automatic Micromeritics ASAP 2020 analyzer based on the Brunauere-Emmette-Teller (BET) gas adsorption method. The sample was outgassed at 300°C for 6 h in a dynamic vacuum before physisorption measurement. The specific surface area was calculated by BET method.

2.2 Electrochemical performance

The electrochemical performance was evaluated in CR2025 coin-type cells. The working electrode was prepared as follows: 60 wt.% of $ZnFe_2O_4$ was mixed with 15 wt.% polyvinylidene difluoride(PVDF) and 25 wt.% acetylene black in N-methyl- 2-pyrrolidone(NMP) solvent to prepare a slurry. The slurry was coated on the Cu foil of 10 μm thickness and then heated in a vacuum oven at 120°C for 12 h, and punched into circular discs. Finally, the electrode was dried under vacuum at 80°C for 10 h. The coin cells were assembled in an argon-filled glove box using lithium foil as the anode, Celgard2400 as the separator, and a mixture of 1.0 M $LiPF_6$ solved in solvents of ethylene carbonate and diethyl carbonate(1:1 vol.%) as electrolyte.

Galvanostatic cycling tests was performed on battery test system(NewareBTS-610) at a current density of 60 mA g^{-1} between 3.0 and 0.01 V (*vs.* Li/Li$^+$). Cyclic voltammetry(CV) and electrochemical impedance spectroscopy(EIS) measurements were conducted on a three-electrode electrochemical cell using electrochemical workstation(Shanghai Chenhua Instrument Co.). where lithium metal foil and wire were used as reference and counter electrodes, separately. CV measurements were performed at a scan rate of 0.1 mV s^{-1} in the voltage range of 0.01-3.0 V (*vs.* Li/Li$^+$), and EIS were recorded with an ac voltage signal of ±5 mV over a frequency range from 10^{-2} to 10^5 Hz. The obtained impedance spectras were fitted based on the ZsimpWin300 Program.

3. RESULTS AND DISCUSSION

3.1 SEM analysis

The SEM figures of $ZnFe_2O_4$ nanomaterials are shown in Fig. 1(a-d).

It is obvious that ZF-500 materials are highly agglomerated. As the annealing temperature increases to 600°C, the morphology of the material has been changed drastically, and the agglomeration is weakened and the grains are spread uniformly.
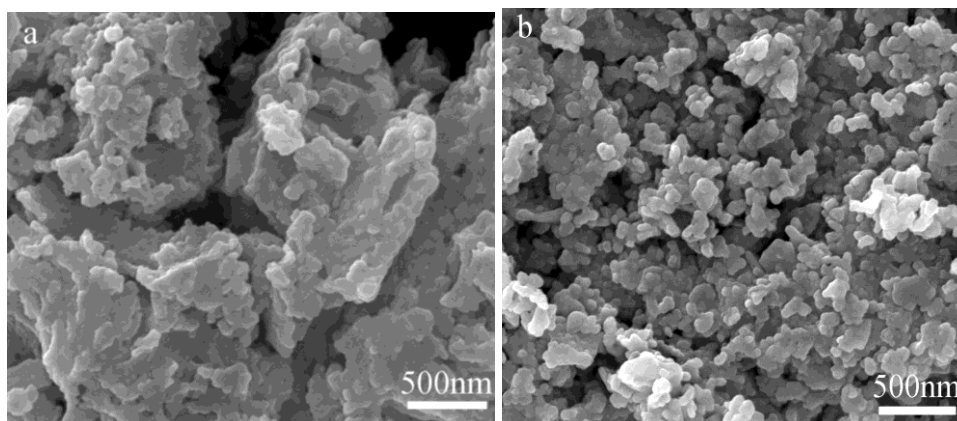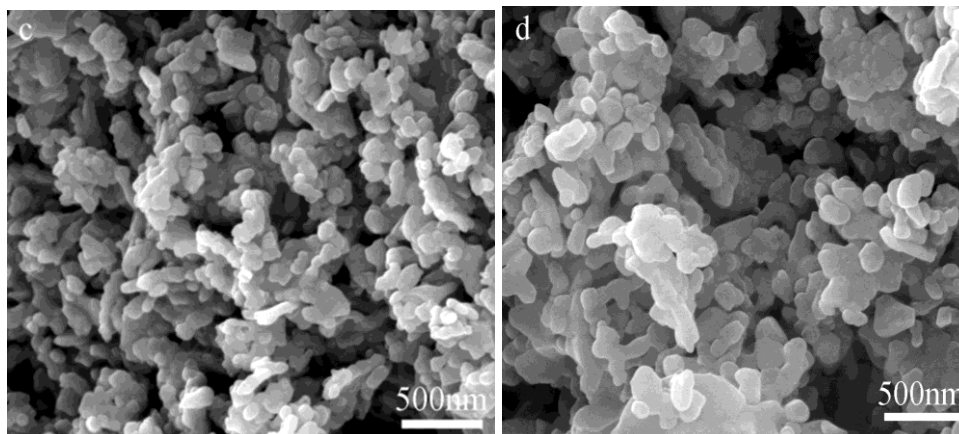
Figure 1. The SEM images for ZF-500 (a), ZF-600 (b), ZF-700 (c) and ZF-800 (d)

Moreover, the size of nanocrystals gradually enhances with increased annealing temperature, which can be ascribed to the improved atomoic diffusion[7], and the rice-shaped particles are gradually appeared from 700 to 800°C.

3.2 XRD analysis

The XRD patterns of ZF-500, ZF-600, ZF-700 and ZF-800 nanoparticles are shown in Fig.2.
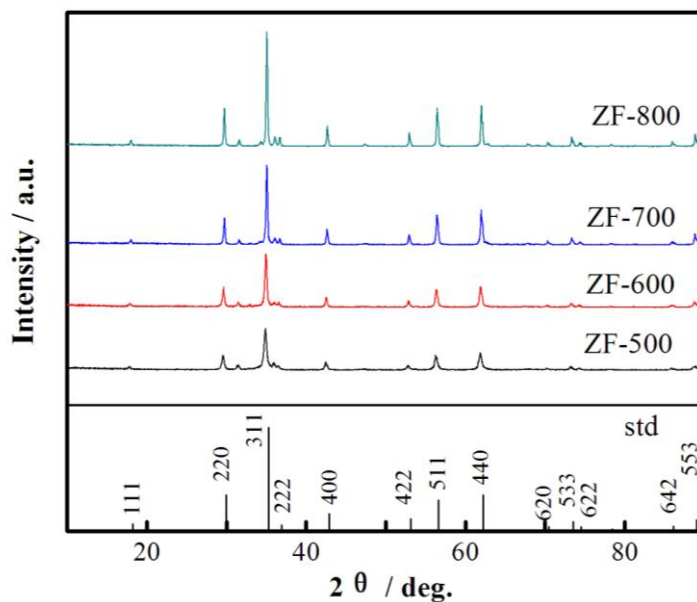
Figure 2. XRD patterns for ZF-500, ZF-600, ZF-700 and ZF-800.

All the reflection peaks can be indexed as $ZnFe_2O_4$ with spinel structure(JCPDS Card #00-022-1020). No peaks attributable to other phases are identified, which indicates the single phase of the zinc ferrite was synthesized. Furthermore, with the increase in sintering temperature, the diffraction

intensity of the peaks increases and the shape of the peaks becomes sharp. These changes show that the $ZnFe_2O_4$ particle after higher temperature sintering is better crystallized. To further investigate the influence of sintering temperature on particle size, the average crystallite sizes of ZF-500, ZF-600, ZF-700 and ZF-800 were acquired from the Scherrer Equation and they are 28.6, 39.0, 43.6 and 50.8 nm, respectively. The average crystallite sizes can be modified by simply adjusting the annealing temperatures.

3.3 BET analysis

The surface area of ZF-500, ZF-600, ZF-700 and ZF-800 was calculated based on Multipoint N_2 adsorption-desorption experiment. The detailed numerical results are showed in Tab.1. we can conclude that the surface area is gradually decreased with the increase of sintering temperature, indicating that the particle size is growing slowly accompanied by the enhanced heated temperature. The result is in accordance with the calculated value of the particle size from the Scherrer Equation.

Table 1. The values of BET surface area of various materials

Samples	ZF-500	ZF-600	ZF-700	ZF-800
$S_{BET}/m^2\,g^{-1}$	49.52	26.99	14.72	8.22

3.4 The electrochemical performance

The electrochemical performance of $ZnFe_2O_4$ electrodes was examined by galvanostatic charge-discharge cycling between 0.01 and 3.0 V at the current density of 60 mA g^{-1}. Fig.3 shows the initial charge-discharge profiles and cycling performance of ZF-500, ZF-600, ZF-700 and ZF-800 electrodes. In Fig.3(a), It can be seen that the initial discharge specific capacities of ZF-500, ZF-600, ZF-700 and ZF-800 electrodes are 1284.4, 1384.4, 982.7 and 963.4 mAh g^{-1}, respectively, and the reversible charge capacities are 979.0, 906.9, 593.1 and 513.0 mAh g^{-1}. The phenomenon of such a high first irreversible capacity loss agrees with the previous reports[1,5], which arises mainly from the incomplete conversion reaction which is deleterious to practical applications[8]. Further work should be investigated in the future. The reversible capacities of ZF-500 and ZF-600 electrodes are conspicuously higher than that of ZF-700 and ZF-800. It may be attributed to the higher reaction activity of particles with higher surface area. Moreover, the coulombic efficiency of ZF-500, ZF-600, ZF-700 and ZF-800 nanoparticles is 76.2%, 65.5%, 60.4% and 53.2% in the first cycle, respetively. The first coulombic efficiency of materials sintered at 500 and 600°C is obviously higher than that at 700 and 800°C.
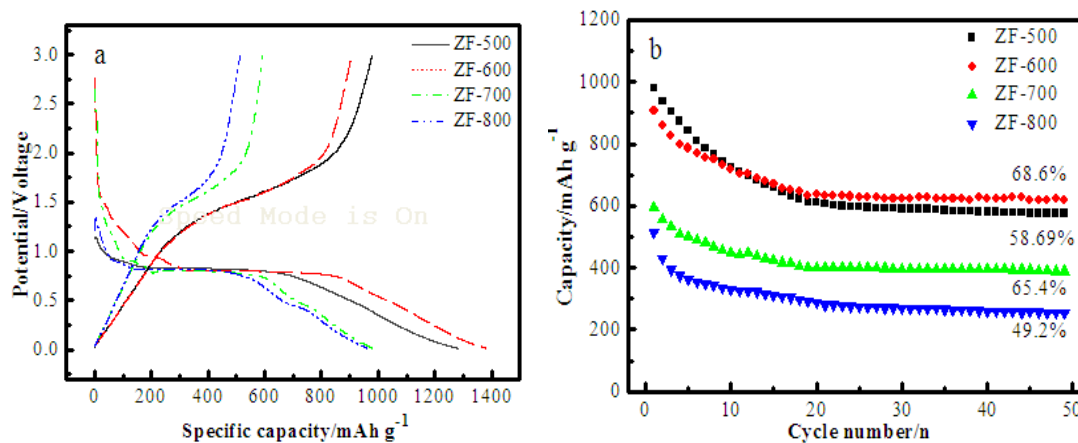
Figure 3. Galvanostatic charge-discharge curves(a) and cycling performance(b) of ZF-500, ZF-600, ZF-700 and ZF-800 electrodes

Fig.3(b) demonstrates the cycling performance of ZF-500, ZF-600, ZF-700 and ZF-800 electrodes. Since the second cycle, the discharge capacity of $ZnFe_2O_4$ electrode decreases obviously, indicative of typical characteristics of discharge capacity trends of transition metal oxide electrode[9,10], and tends to become steady after 20 cycles. It is worthy mentioning that the ZF-600 sample still manifests the highest capacity(622.5 mAh g^{-1}) and capacity retention(68.6%) after 50 cycles. The specific capacity and the capacity retention are shown in Tab.2. This may be ascribed to the multiple impacts including small particle size, high crystallinity and superior dispersibility.

Table 2. The capacity and the capacity retention of the samples

Sample	1st charge capacity/ mAh g^{-1}	50th charge capacity/ mAh g^{-1}	The capacity retention /%
ZF-500	979.0	575.2	58.8
ZF-600	906.8	622.5	68.6
ZF-700	593.1	387.6	65.4
ZF-800	513.0	252.2	49.2

$ZnFe_2O_4$ materials sintered at various temperatures were also characterized by cyclic voltammetry (CV), and it is presented in Fig.4. There is an obvious difference between the first and the subsequent cycles. In the first cycle, two minor peaks can be observed at about 1.5 and 1.2 V, followed by a more pronounced peak at around 0.85 V, and finally the main sharp reduction peak at around 0.6V. These irreversible cathodic peaks represent the initial reduction reaction of $ZnFe_2O_4$. It is proposed that $ZnFe_2O_4$ would be initially lithiated to $Li_xZnFe_2O_4$ (0＜X≤2) in the potential above 0.6 V, the peak at 0.6 V is corresponding to the reduction of Zn(II) and Fe(III) to their metallic states, and the peak below 0.6 V can be related to Li-Zn alloying reaction[11]. It should be noted that the variation in the intensity and position of the above reduction peaks is usually related to lithiation extent within

the solid solution domains, which would likely vary for different particle sizes, shapes and crystallization degrees.
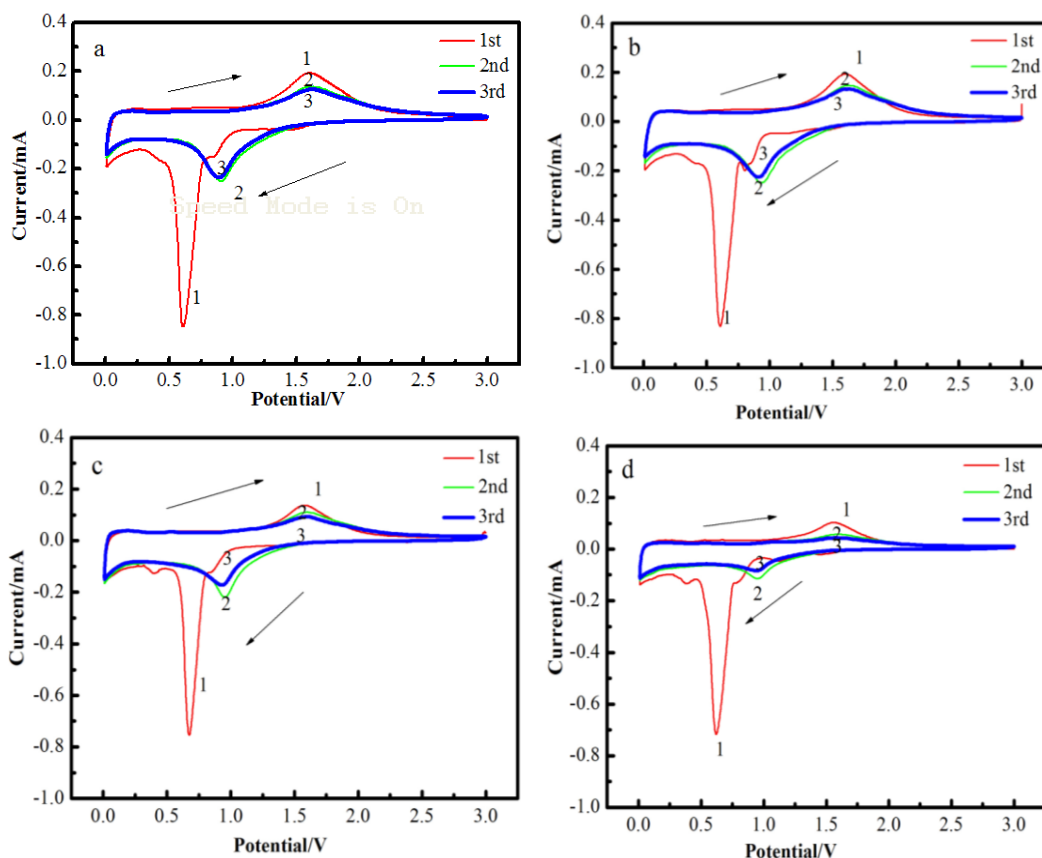
Figure 4. The Cyclic voltammograms of ZF-500(a), ZF-600(b), ZF-700(c) and ZF-800(d) electrodes

After the first scan, these peaks disappear and are displaced by a new peak located at 0.91V, indicating that the reversible reduction reaction of Fe_2O_3 and ZnO. The anodic peak located at 1.6V in the first cycle does not obviously shift in the subsequent cycles, which is ascribed to the oxidation of the metallic iron and zinc into Fe(III) and Zn(II), respectively[8,12]. Also, the wide oxidation peaks at 0.10 V is identical with the Li^+ de-alloying from the Li-Zn alloying and de-intercalation[13]. Furthermore, the oxidation and reduction peak current and peak area of ZF-700 and ZF-800 electrodes are significantly lower than ZF-500 and ZF-600 electrodes, indicating that the electrochemical activity of the former two materials is weaker, especially for the ZF-800 material. These are in accordance with the charge/discharge performance.

Electrochemical impedance spectroscopy has been carried out to investigate the difference in electrochemical performance for $ZnFe_2O_4$ electrodes prepared at various temperatures. The measurements were carried out in the discharged state of 0.01 V at 50th cycles. The measured impedance spectras and the corresponding fitted impedances based on the equivalent circuit[14] are presented in Fig. 5(a). The intercept at the real (Z') axis in high frequency represents the ohmic resistance(R), the semicircle in the middle frequency range are respectively the constant phase element

(CPE) and charge transfer resistance (R_{ct}) at the electrode/electrolyte interface, and a straight sloping line at the low frequency region of the Nyquist plots indicates the diffusion of ions in the bulk electrode(Z_w).
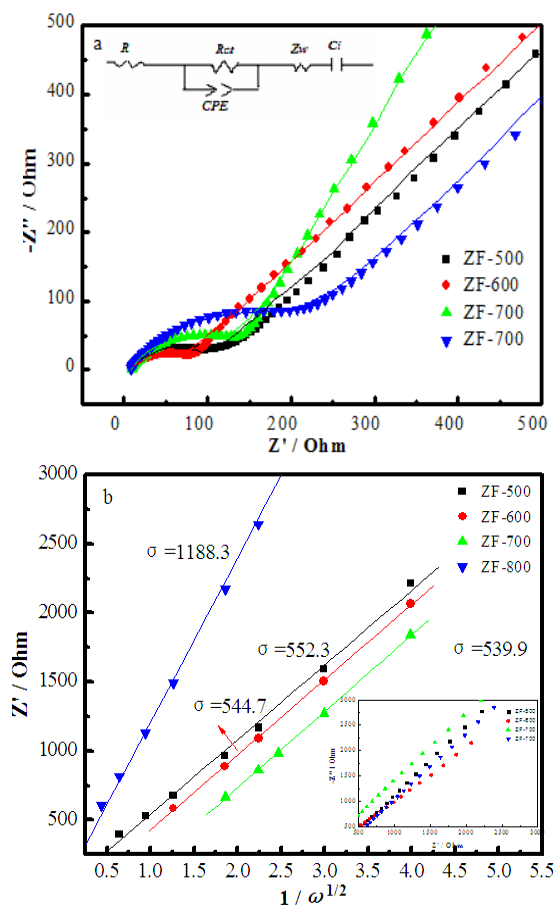
Figure 5. Electrochemical impedance spectroscopy and equivalent circuit(a), and the corresponding plots of Z_{re} vs. $\omega^{-1/2}$ at low frequency region(b) of ZF-500, ZF-600, ZF-700 and ZF-800 electrodes

The R_{ct} values are obtained based on the fitted impedances(solid line in Fig.5(a)) using the proposed equivalent circuit. The R_{ct} for ZF-500, ZF-700 and ZF-800 electrodes are 73.9，106.4 and 177.9 Ω, respectively, while only 43.9 Ω for ZF-600. Clearly, a fast lithium intercalation kinetic process is occurred at the surface of $ZnFe_2O_4$ electrode sintered at 600°C, related to the characteristic of the higher reactivity activity of the material.

Furthermore, the diffusion coefficient of lithium ion can be calculated according to the following formula[15,16]:

$$D = \frac{R^2T^2}{2A^2n^4F^4C^2\sigma^2} \qquad (1)$$

where R is the gas constant, T is the absolute temperature, n is the number of reacting electron per molecule, A is the area surface of the electrode, F is the Faraday constant, C is the molar concentration of Li$^+$, D is the diffusion coefficient, and σ is the Warburg coefficient, calculated from the slope of the Z' *vs* $\omega^{-1/2}$ linear plot obtained in the low frequencies region. The plots of Z_{re} *vs.* $\omega^{-1/2}$ at low frequency region for ZnFe$_2$O$_4$ electrodes were shown in Fig.5(b) and the insets were Nyquist plots in the low frequency range. The lithium diffusion coefficients in ZF-500, ZF-600, ZF-700 and ZF-800 electrodes are calculated to be 1.33×10^{-15}, 2.01×10^{-15}, 9.44×10^{-16} and 1.34×10^{-16} cm^2 s^{-1}. The higher diffusion capability of ZnFe$_2$O$_4$ annealed at 600°C originates from the smaller particle size and better dispersibility, which is the essential reason for the optimum electrochemical performance of ZF-600 electrode.

4. CONCLUSION

Annealing temperature dependent on morphology and electrochemical properties of ZnFe$_2$O$_4$ nanoparticles synthesized by sol-gel method has been demonstrated. The nanomaterial sintered at 600°C shows the higher capacity and better cycling stability. The material treated at 600°C exhibits the initial reversible capacity of 1384.4 mAh g^{-1}, much higher than that sintered at 800°C, 963.4 mAh g^{-1}, and after 50 cycles, the former retains the capacity retention of 68.6%, dramatically above the latter, 49.2%. It is attributed to the uniform appearance and moderate particle size, which facilitates the faster lithium ion transport due to the low charge transfer resistance and high lithium diffusion coefficient. The temperature control is an important preparing condition of the electrode material affecting the electrochemical behavior.

References

1. L. Lin, Q.M Pan, *J. Mater. Chem.,* A 3 (2015) 1724-1729.
2. X.Q. Tang, X.H. Hou, L.M. Yao, S.J. Hu, X. Liu, L.Z. Xiang, *Mater. Res. Bull.,* 57 (2014) 127-134.
3. M.Y. Wang, L. Sun, J.H. Cai, P. Huang, Y.F. Su, C.J. Lin, *J. Mater. Chem.,* A1 (2013) 12082-12087.
4. D. Narsimulu, B. Nageswara Rao, M. Venkateswarlu, E.S. Srinadhu, N. Satyanarayana, *Ceram. Int.,* 42(2016) 16789-16797.
5. A.S. Hameed, H. Bahiraei, M.V. Reddy, M.Z. Shoushtari, J.J. Vittal, C.K. Ong, B.V.R. Chowdari, *ACS Appl. Mater. Inter.,* 6 (2014) 10744-10753.
6. H. Hwang, H. Shin, W.J. Lee, *Sci. Rep.,* 7 (2017) 1-10.
7. G. Li, X.B. Zhu, W.H. Song, Z.R. Yang, J.M. Dai, Y.P. Sun, *J. Am. Ceram. Soc.,* 94 (2011) 2872-2877.
8. F. Zou, X.L. Hu, Z. Li, L. Qie, C.C. Hu, R. Zeng, Y. Jiang, Y.H. Huang. *Adv. Mater.,* 26 (2014) 6622-6628.

9.   Q.H. Wu, R.F. Zhao, X. Zhang, W.L. Li, R.H. Xu, G.W. Diao, M. Chen, *J. Power Sources,* 359 (2017) 7-16.
10. S.H. Yu, S.H. Lee, D.J. Lee, Y.E. Sung, T. Hyeon, *Small,* 11 (2015) 1-27.
11. D. Bresser, E. Paillard, R. Kloepsch, S. Krueger, M. Fiedler, R. Schmitz, D. Baither, M. Winter, S. Passerini, *Adv. Energy Mater.,* 3 (2013) 513-523.
12. L.M. Yao, X.H. Hou, S.J. Hu, J. Wang, M. Li, C. Su, M.O. Tade, Z.P. Shao, X. Liu, *J. Power Sources,* 258 (2014) 305-313.
13. Y. Wang, Y.H. Jinb, R.P Zhang, M.Q. Jia. *Appl. Surf. Sci.,* 413 (2017) 50-55.
14. H.Y. Xu, X.L. Chen, L. Chen, L.E. Li, L.Q. Xu, J. Yang, Y.T. Qian, *Int. J. Electrochem. Sci.,* 7 (2012) 7976-7983.
15. C. Hwang,T. Kim, J. Shimc, K. Kwaka, K.M. Ok, K.K. Lee, *J. Power Sources,* 294 (2015) 522-529.
16. R.J. Meng, H.Y. Hou, X.X. Liu, C.X. Yan, J.X. Duan, S. Liu, *Ceram. Int.,* 42 (2016) 6039-6045.